

# Multilayer Reflection Tomography from Monte Carlo Simulations

Rasmus B. Nielsen<sup>\*a</sup>

Submitted June 2018, accepted July 2018

X-ray Reflection Tomography (XRT) is a tool for imaging of buried layers and interfaces in multilayer thin-films. The method combines X-ray reflectivity and computerized tomography to determine spatially dependent reflectivity curves.<sup>1–3</sup> Simulations of X-ray reflection tomography experiments make it possible to assess to which accuracy properties can be determined and evaluate various reconstruction methods.<sup>2</sup> It is thus important that such simulations mimic real experiments. In this paper it is shown that a Monte Carlo approach can be used to simulate XRT experiments and test reconstruction techniques. This approach takes into account the statistical properties of an experimental X-ray setup and allows for simulation of diverse experimental configurations. The currently used analytical simulations based on projections do not include such statistics and are limited in scope. The Monte Carlo approach will facilitate further development of the applications of XRT.

## 1 Introduction

X-ray reflectivity is an outstanding tool for non-destructive determination of the structure of thin multilayer structures. The main advantage is that the reflected intensity depends on features of the layer thickness at nanoscale. These multilayer thin films are used e.g. for energy storage, in photonics and in many semiconductor devices such as batteries, LEDs, MEMS, superlattices, etc. Deposition techniques allow the multilayer materials to be tailor-made with layer thicknesses at the atomic scale. To analyze and assess the quality of such materials a technique with sensitivity at a scale of similar length is required.<sup>4</sup>

Reflectivity is measured by the intensity of specular reflection as a function of wavevector transfer ( $Q$ ). This is done by keeping the X-ray energy constant and varying the incident angle close to grazing incidence as shown in Figure 1.  $Q$  is a vector equal to the difference between the vector describing the incoming wave and the scattered wave, for measurements of specular reflection only the magnitude of  $Q$  is of interest:<sup>4</sup>

$$Q = \frac{4\pi}{\lambda} \sin(\theta) \quad (1)$$

Up to a certain angle i.e. the critical angle, X-rays experience total external reflection because the index of refraction in the X-ray regime is lower in solids than in air.

Beyond this angle the reflectivity is determined by Kiessig fringes caused by interference of the scattered X-rays from the different interfaces in the sample.<sup>4,5</sup> As a function of  $Q$ , the reflectivity depends on electron density, the layer thickness and roughness of interfaces between layers. The measured reflectivity curve can thus be used to determine all these multilayer properties. For normal X-ray reflectivity (XRR), however, only the average reflectivity is recorded so the determined properties are also averages of the illuminated portion of the sample.<sup>6</sup>

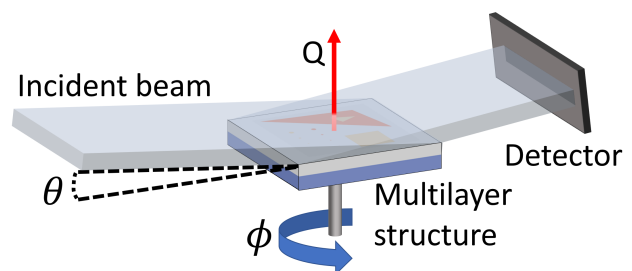


**Fig. 1** XRT setup: A sinogram at constant  $Q$  is created by keeping the incident angle  $\theta$  constant while changing the in-plane angle  $\phi$ .

### 1.1 Parratt's recursive method

To calculate the reflectivity as a function of  $Q$  for a given multilayer structure, the kinematical approximation or Par-

<sup>a</sup> Copenhagen, Denmark. E-mail: fbg450@alumni.ku.dk

ratt's recursive method is usually applied. While being easier to use the kinematical approximation is only valid at a high  $Q$  and fails completely near and below the critical wavevector. Since reflectivity in this case is measured from below and past the critical wavevector, Parratt's recursive method is required. This method uses the refractive index and the Fresnel relation to determine the reflectivity from a single interface. The reflectivity is then calculated from the bottom interface and up. Since there are no reflections from below the bottom interface, the reflected intensity can be determined as a function of the intensity reaching this interface, the refractive index of the materials at this interface and  $Q$ . The reflectivity of the next layer can now be determined, since the reflectivity of the layer below is known. This can be continued recursively until the reflectivity of the entire multilayer structure is known.<sup>4,7</sup>

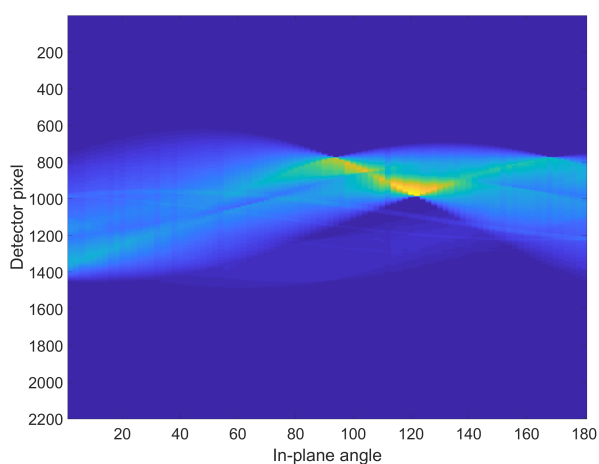


**Fig. 2** Sinogram at  $Q = 0.0976 \text{ \AA}^{-1}$  generated from 90 measurements in McXtrace. It was used to reconstruct the spatially dependent reflectivity at this  $Q$ -value, as shown on Figure 4.

## 1.2 X-ray reflection tomography

X-ray reflection tomography (XRT) combines many reflectivity measurements from various sample orientations by applying computerized tomography.<sup>1-3</sup> This enables determination of the spatial dependence of the reflectivity curve.<sup>1</sup> X-ray reflectivity is typically measured at incident angles of a few milliradians, thus the height of the reflected beam along the  $Q$ -vector is in the 10 - 100  $\mu\text{m}$  range for typical sample sizes. This is too small to separate intensity from different parts of the sample along the direction of X-ray propagation. The measured intensity is thus the sum of all reflected intensities along the propagation direction. With a collimated beam, the width of the reflected beam running parallel to the sample surface is equal to the width of the illuminated area of the sample.

By measuring the reflectivity with a collimated monochromatic beam at different in-plane angles ( $\phi$ ), it is possible to combine the results into a sinogram of the sample at constant  $Q$  as shown in Figure 2. By using computerized tomography on the sinogram, it has been shown that the spatially dependent reflectivity can be determined at constant  $Q$ .<sup>1</sup> By measuring sinograms at different incident angles, the entire spatially resolved reflectivity curves can be determined. By applying XRT in this manner it has been shown that the tomography can be reconstructed and used to determine heterogeneous layer thickness locally. This is done by fitting analytical solutions from Parratt's recursive method to the measured reflectivity curves.<sup>1</sup> A spatially dependent reconstruction from a sinogram can be achieved by the methods listed below.

### 1.2.1 Filtered back projection

Reconstruction can be obtained through filtered back projection (FBP) since the Fourier transform of projections in real space is equal to slices of the Fourier space. By combining multiple slices and applying a high-pass filter the real space tomography of the sample can be reconstructed.<sup>2-4</sup> The FBP method has the advantage that it is computationally efficient, but the required use of a high-pass filter results in increased noise. This noise increase is troublesome if the reflectivity in a small area of the sample is to be determined, such as by micro X-ray reflectivity ( $\mu\text{XR}$ ).

### 1.2.2 Algebraic reconstruction techniques

Algebraic reconstructions techniques (ART) are based on solving the inverse problem of the system of linear equation given by:

$$\mathbf{A}\vec{x} = \vec{b} \quad (2)$$

Where  $\vec{x}$  is the spatially dependent reflectivity of the sample.  $\vec{b}$  contains the observed intensities in the form of a vector representation of the sinogram.  $\mathbf{A}$  describes the dependence of observations on the reflectivity of the sample. The components of  $\mathbf{A}$  are so-called line-pixel coefficients, which describe how an X-ray beam interacts with the sample before hitting the detector. To determine  $\vec{x}$  it is necessary to calculate an approximation of the inverse of  $\mathbf{A}$ .  $\mathbf{A}$  can be calculated analytically, but determining the inverse of  $\mathbf{A}$  is not a straightforward task for systems using detectors operating with thousands of pixels. ART methods are thus more demanding to compute than FBP but allow for more corrections, such as constraining the reflectivity so it doesn't use unrealistic values.<sup>8,9</sup> ART is especially useful when only limited data are available to reconstruct the tomography.

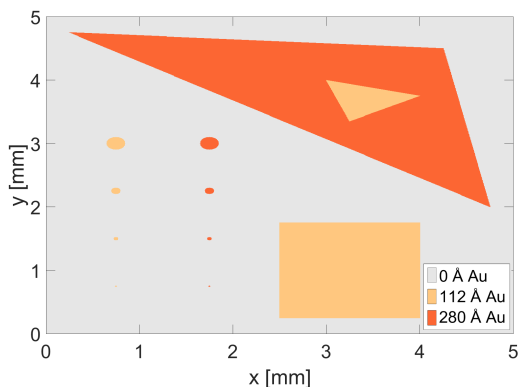


**Fig. 3** Map of the heterogeneous multilayer phantom used in simulations. The map assigns each position a reflectivity curve corresponding to the multilayer structure, this means reflectivity is a function of  $x$ ,  $y$  and  $Q$ . A map with sharp edges was chosen because these tend to be harder to reconstruct. The circles to the left side of the map have a diameter of  $200\mu\text{m}$ ,  $100\mu\text{m}$ ,  $50\mu\text{m}$  and  $20\mu\text{m}$  (from the top). They have been included to explore the achievable resolution.

## 2 Simulations

Simulations were based on simulating a XRT experimental setup with Monte Carlo algorithms. The Monte Carlo methods allow for simulation of systems with statistics corresponding to realistic experiments if the probability distributions of these systems are known. McXtrace<sup>10</sup> is a Monte Carlo environment for simulating X-ray experiments by using a ray-tracing technique where every single photon is created with position and wavelength based on the probability distribution of the source. The propagation of each photon is determined by calculating how it interacts with the components it passes.<sup>10</sup> For the purpose of using McXtrace for XRT simulations, the author has created a new heterogeneous multilayer component. McXtrace already included a homogeneous multilayer component that determined the specularly reflected intensity from kinematic calculations or from a reflectivity curve.<sup>10</sup> The new component mapped different positions on the sample to different reflectivity curves. This was done by initially reading an input map file by extending the embedded C-code in McXtrace. Whenever a photon hit the sample the impact position was used to determine which reflectivity curve to use. Subsequently, the existing multilayer component was called by using McXtrace's meta-language, but with the reflectivity curve corresponding to the position on the map.

To determine whether the simulations correlated with real experiments, the materials from "Interface-sensitive imaging by an image reconstruction aided X-ray reflectivity technique"<sup>1</sup> were simulated in a synchrotron setup

matching the one used in the experiment. The simulated multilayer was a Si substrate with an Au layer of varying thickness underneath a layer of Ti. The exact layout of the multilayers of the sample is shown in Figure 3. Reflectivity curves of the simulated multilayer structures were first simulated in GenX<sup>11</sup>, then the reflectivity curves were used as input for McXtrace. The simulated reflectivity curves are shown in Figure 5. The Parratt recursion formula was used in GenX since the kinematic approach does not take into refraction account, which is needed for total external reflection.<sup>4</sup>

A complete reflectivity tomography dataset was recorded by measuring sinograms with in-plane angle increments of  $2^\circ$  from  $2^\circ$  to  $180^\circ$ . Only a half circle was measured since the angles from  $182^\circ$  to  $360^\circ$  would be essentially the same measurements with mirrored results. For each of these 90 measurements in a sinogram,  $10^8$  photons were simulated. 90 sinograms were simulated at incident angles varying linearly from  $0.108^\circ$  to  $0.464^\circ$ , corresponding to a  $Q$  from  $0.0308 \text{ \AA}^{-1}$  to  $0.1317 \text{ \AA}^{-1}$  at 16 keV. This means that the angle of total external reflection for Au is within the simulated angles as it is at  $Q = 0.08 \text{ \AA}^{-1}$ .<sup>4</sup> The simulated setup was an X-ray beam from a wiggler monochromized to 16 keV with an energy resolution of  $10^{-4}$  keV.<sup>1</sup> This small energy interval was necessary to assume measurement of the reflectivity from each reconstruction was done at constant  $Q$ . A reconstruction was made for each of the 90 sinograms since each sinogram had a single corresponding  $Q$  value. This made it straightforward to compare the simulated reflectivity with that from the analytical solution in GenX.

The original synchrotron experiment was performed by using a detector with a pixel size of  $6.45 \mu\text{m}$  and a beam with a horizontal divergence of  $0.02 \text{ mrad}$ .<sup>1</sup> Simulation of the experiment with McXtrace was performed by assuming a collimated beam. Subsequently, the reconstructions were compared with a reconstruction from a simulation using a fan beam with a horizontal divergence of  $0.02 \text{ mrad}$  in McXtrace. The purpose of this was to show that using a collimated beam was a good assumption. The fan beam was approximated as an infinite number of point-sources with a horizontal divergence given by a Gaussian with an uncertainty of  $0.02 \text{ mrad}$ . The exact beam and divergence profile depend on the source and optics used in the experimental setup. However, just like in the original experiment, it was assumed that there was no vertical divergence.

The reconstructions were achieved by means of both filtered back projection (FBP) and a sub-class of the algebraic reconstruction technique (ART) termed simul-

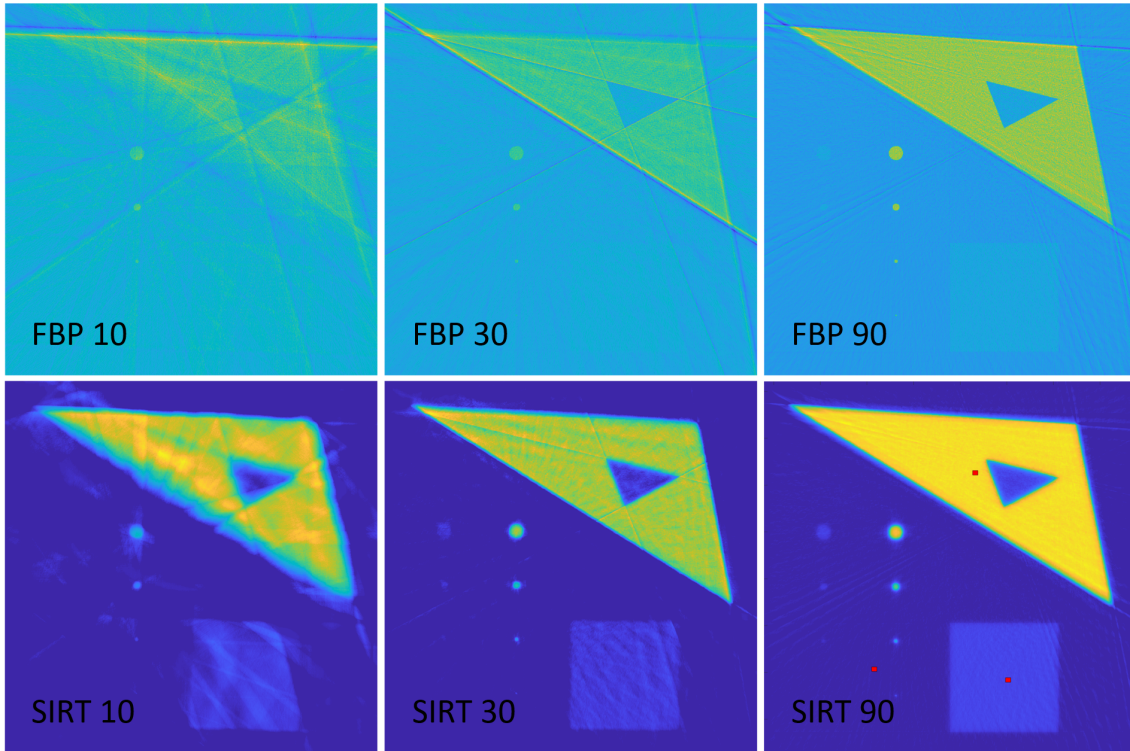


**Fig. 4** Reconstructions of the phantom at  $Q = 0.0976 \text{ \AA}^{-1}$  using FBP or SIRT with 10, 30 or 90 equally spaced projections. The reconstructions performed by means of SIRT show improved signal to noise ratio and fewer artifacts when compared with the reconstructions performed with FBP. The reflectivity curves for Figure 5 are the values at the three red dots in the image of the SIRT reconstruction from 90 projections. Note the pixel size is  $6.45 \mu\text{m}$ , but the red dots are considerably larger to make them visible.

taneous iterative reconstruction technique (SIRT). SIRT is a method that updates every iteration by multiplying the error in the previous iteration with the sums of the columns and rows of  $\mathbf{A}$  simultaneously.

$$\vec{x}_{k+1} = \vec{x}_k + \omega_k \cdot \mathbf{D}^{-1} \cdot \mathbf{A}^T \cdot \mathbf{M}^{-1} \cdot (\vec{b} - \mathbf{A} \cdot \vec{x}_k) \quad (3)$$

$\omega_k$  is a scalar,  $\mathbf{D}$  and  $\mathbf{M}$  are dependent on the ART method used. For SIRT,  $\mathbf{D}$  is a diagonal matrix with the sum of each column of  $\mathbf{A}$  as the diagonal elements, and  $\mathbf{M}$  is a diagonal matrix with the sum of each row of  $\mathbf{A}$  as the diagonal elements. For each iteration the artifacts from reconstruction are reduced, but noise from the measurements also becomes more significant. The optimal number of iterations to use is dependent on the tomography, the experimental setup, the nature of the noise and the exact reconstruction algorithm used. A good stopping rule will terminate the reconstruction when a minimum in noise is obtained.<sup>8,12–16</sup> Determining a stopping rule is a challenging task so a trial and error approach was used to select 150 iterations in the reconstructions: at this number of iterations the exact amount of iterations made minute difference.

### 3 Results and Discussion

To compare the effect on reconstruction quality from the number of projections in each sinogram, the phantom was reconstructed from 10, 30 and the full 90 projections, as shown in Figure 4. All reconstructed phantoms show the patterns from the map. For the full number of projections the reconstruction produces a clear match with the original map of the sample. It is thus shown that the simulated photons have successfully interacted with the heterogeneous sample. The pixel size is  $6.45 \mu\text{m}$ , but a multilayer structure needs to extend to a larger area before the reflectivity matches the original reflectivity curve. Pixels in the center of the circles with a diameter of  $200 \mu\text{m}$  match the reflectivity curves corresponding to the multilayer structure. The structure of the smaller circles was observable only as irregularities in the reflectivity of the surrounding structure. To create better reconstructions, the number of projections or the pixel density of the detector could be increased. Both of these would lead to more measurements, which would produce a reconstruction in a better quality.

To show that the method can be used to test reconstruction techniques, the reconstructions from the different

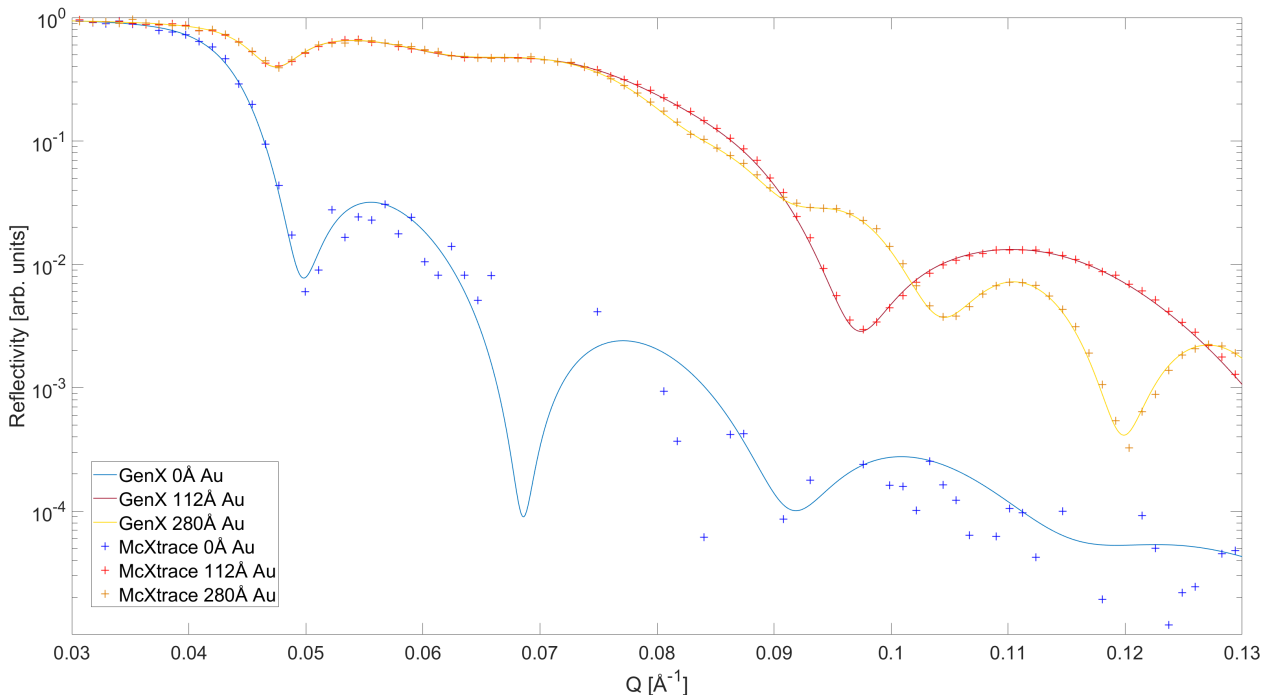


**Fig. 5** The reconstructed reflectivities in single pixels of sidelength  $6.45 \mu\text{m}$  show a high degree of correlation with original reflectivity curves. The position of the three pixels can be seen in Figure 4. All the reflectivity data from McXtrace has been multiplied with the same value to obtain the same reflectivity as for GenX for  $Q = 0.0308 \text{ \AA}^{-1}$ . A similar value could also be obtained by extrapolating the curves to  $Q = 0$ . This is justified because the reflectivity should always approach 1 as  $Q$  approaches 0. The critical angle of Au is clearly visible as a high reflectivity until  $Q = 0.08 \text{ \AA}^{-1}$ . At low reflectivity the uncertainty from artifacts in the reconstruction and the limited photon count in the Monte Carlo method dominates.

amount of projections were compared. As expected, missing information caused the greatest effect on the FBP reconstructions, as can be seen in the number of artifacts. Especially the thinner  $112 \text{ \AA}$  layer of Au becomes hard to distinguish since areas with higher contrast create artifacts with more intensity.

The reflectivity at individual positions (micro X-ray reflectivity,  $\mu\text{XR}$ ) was determined by plotting the reflectivity as a function of  $Q$ .<sup>6</sup> This is compared with the initial reflectivity curves in Figure 5. It is evident from the reconstruction that it is possible to determine which of the three multilayer structures the chosen pixels belong to.

To get a quantitative overview of the differences between the qualities of the reconstructions, Mander's overlap coefficient (MOC) was calculated. The purpose was to show that using SIRT with 150 iterations delivered a good reconstruction as shown in Figure 6. Another purpose was to show that the quality of the SIRT reconstruction was superior to that of the FBP. MOC is given

by:<sup>17</sup>

$$r = \frac{\sum_i s1_i \cdot s2_i}{\sqrt{\sum_i (s1_i)^2 \cdot \sum_i (s2_i)^2}} \quad (4)$$

$s1_i$  was the reflectivity value of a pixel on the map as determined from the reflectivity curve corresponding to the material assigned to that position on the map.  $s2_i$  was a weighted average of the reflectivities in the reconstruction that shared position with the map pixel. The weights were equal to the amount of overlap. A weighted average was required because the reconstructions might not have the same pixel position or size as the map.

The reflectivity of all pixels for all 90 incident angles  $\theta$  were summed up and compared using MOC. A MOC of 1 means the reconstructions correlate perfectly with the map and the reflectivity curves, whereas a MOC of 0 means there is no correlation.<sup>17</sup> This was possible because the perfect result was known in the form of the reflectivity curves of the materials from GenX. The map used as input for McXtrace then assigned these materials to known positions. This was an advantage of using simulation since a reconstruction from experiment would require another

type of experiment with higher precision to determine the quality of a reconstruction. Using all 90 projections, the SIRT reconstruction with 150 iterations had a MOC of 0.993 whereas the reconstruction using FBP had 0.953. Comparison between SIRT and FBP for a different number of projections is shown in Figure 7. The SIRT reconstruction from a beam with a horizontal divergence of 0.02 mrad also had a MOC of 0.993, which shows that a collimated beam produced a good approximation.

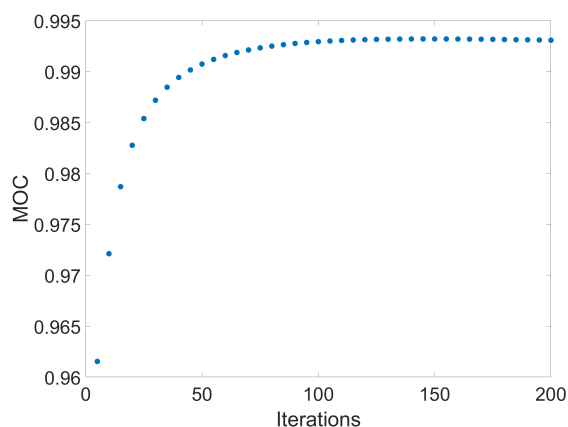


**Fig. 6** SIRT reconstruction quality as a function of iterations shows that at 150 iterations the change in quality per iteration is minimal. MOC begins decreasing after approximately 150 iterations, which is why this number of iterations was chosen. MOC is calculated at every 5 iterations using all 90 projections.

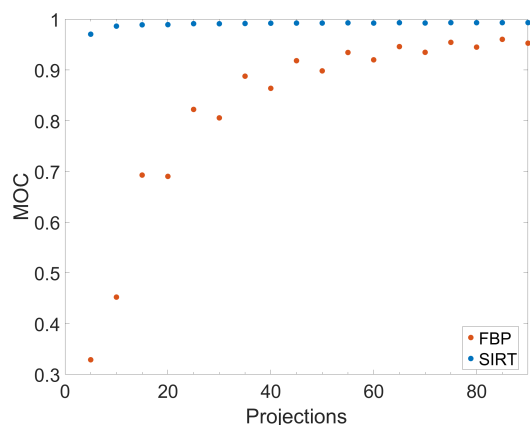


**Fig. 7** MOC as a function of the number of equally spaced projections used in the reconstruction. SIRT is clearly the better match to the original reflectivity curves, especially with a small number of projections. Oscillatory behavior occurs because some directions are more important than others for calculating the best reconstruction. MOC is calculated at every 5 equally spaced projections.

McXtrace returns errors on the detector intensities

from the necessary use of a limited number of photons. Reconstruction of these errors using SIRT gave an estimate of errors arising from the Monte Carlo approach. This resulted in an uncertainty in the  $\mu$ XR curves in the order of  $10^{-2}$  decreasing to  $10^{-4}$  as  $Q$  is increased. This together with the artifacts from the reconstruction and the bandwidth of the beam is the source of any uncertainties in the  $\mu$ XR curves. Error bars are omitted since the exact contribution from artifacts is undetermined and depends on the positions as well as the exact reconstruction algorithm used. In real experiments uncertainty also arises from dispersion of the beam, which affects the incident angle and thus the magnitude of  $Q$  for the interaction. The lateral size of the evanescent wave means that a photon hitting the sample in a heterogeneous area will interact with several multilayer structures. This effect was not included in the simulations since only one reflectivity curve was used for any one photon. The effect of diffuse scattering from rough interfaces to other areas of the detector was not included in the simulations. However, diffuse scattering contributes significantly less than specular reflection. The reconstructed reflectivity curves for areas with low reflectivity might be affected by diffuse scattering from other areas of the sample.

## 4 Conclusions

Based on the full reflectivity dataset it has been shown that the Monte Carlo approach produces results which can be used to test reconstruction techniques. Since the optimal result is known, it is possible to calculate measures to quantitatively evaluate the reconstruction quality. The reconstruction has shown that there is a contrast between different areas and that it is possible to determine where the thickness of a layer changes. The  $\mu$ XR curves show that it is possible to determine the reflectivity as a function of both position and wavevector transfer. This means that the tomography of the phantom can be determined and it shows that the simulations return the expected results. The use of Monte Carlo simulations produce more realistic noise, and it is possible to add more factors, as deemed necessary. By using the McXtrace environment, it is possible to change the source characteristics, the optics and the detector. This can be achieved by using the already included components or by adding new ones.

### 4.1 Outlook

During the continued development of these simulations it will be important that the noise generated corresponds to real experimental noise. That way, the simulations can be used to determine optimal experimental setups and reconstruction techniques and to get an idea of the image quality

---

to be expected from these experiments. When this is considered, it will be a stepping stone towards creating optimal XRT experiments on lab-source experimental setups.

## 5 Acknowledgments

I would like to express my gratitude to all the people who have assisted me in this project: My supervisor and professor Kell Mortensen for agreeing to this project, for always having time when I passed by, and for answering my questions. My external supervisor Erik Lauridsen for coming up with the idea for this project, for providing the contacts needed to answer some of the challenging questions that arose during the project, and for making sure that I stuck to the schedule. Erik Knudsen from DTU for giving insight into McXtrace, for giving ideas on how to make a new component and for providing the computational resources needed to run the simulations. Professor Per Hansen from DTU for providing access to algebraic and reconstruction tools and the documentation needed to understand these. The Xnovo team for helping me with the software needed in this process. Finally, thank you to Karenlise Nielsen for providing professional linguistic assistance and for providing the initial contact that started all this.

## References

- 1 J. Jiang, K. Hirano and K. Sakurai, *Journal of Applied Crystallography*, 2017, **50**, 712-721.
- 2 V. A. Innis-Samson, M. Mizusawa, K. Sakurai, *Adv. X-Ray. Chem. Anal., Japan* 2012, **43**, 391-400.
- 3 V. A. Innis-Samson, M. Mizusawa and K. Sakurai, *Analytical chemistry*, 2011, **83**, 7600-7602.
- 4 J. Als-Nielsen and D. McMorrow, *Elements of Modern X-ray Physics*, John Wiley & Sons Ltd, Chichester, 2011.
- 5 H. Kiessig, *Annalen der Physik*, 1931, **402**, 769-788.
- 6 S. Kenji, M. Mari, I. Masashi, K. Shun-ichi and I. Yasuhiko, *Journal of Physics: Conference Series*, 2007, **83**, 012001.
- 7 L. G. Parratt, *Physical Review*, 1954, **95**, 359-369.
- 8 P. C. Hansen and J. S. Joergensen, *Numerical Algorithms*, 2017, DOI: 10.1007/s11075-017-0430-x.
- 9 R. Gordon, R. Bender, G. T. Herman, *Journal of theoretical biology*, 1970, **29**, 471-481.
- 10 E. Bergbäck Knudsen, A. Prodi, J. Baltser, M. Thomsen, P. Kjær Willendrup, M. Sanchez Del Rio, C. Ferrero, E. Farhi, K. Haldrup, A. Vickery, R. Feidenhans'l, K. Mortensen, M. Meedom Nielsen, H. Friis Poulsen, S. Schmidt and K. Lefmann, *Journal of Applied Crystallography*, 2013, **46**, 679-696.
- 11 M. Björck and G. Andersson, *Journal of Applied Crystallography*, 2007, **40**, 1174-1178.
- 12 P. Gilbert, *Journal of theoretical biology*, 1972 **36**, 105-117.
- 13 A. van Der Sluis and H. A. van Der Vorst, *Linear Algebra and its Applications*, 1990, **130**, 257-303.
- 14 W. van Aarle, W. J. Palenstijn, J. Cant, E. Janssens, F. Bleichrodt, A. Dabravolski, J. De Beenhouwer, K. J. Batenburg and J. Sijbers, *Optics Express*, 2016, **24**, 25129-25147.
- 15 W. van Aarle, W. J. Palenstijn, J. De Beenhouwer, T. Altantzis, S. Bals, K. J. Batenburg and J. Sijbers, *Ultramicroscopy*, 2015, **157**, 35-47.
- 16 W. J. Palenstijn, K. J. Batenburg and J. Sijbers, *Journal of Structural Biology*, 2011, **176**, 250-253.
- 17 E. M. Manders, F. J. Verbeek, J. A. Aten, *Journal of Microscopy*, 1993, **169**, 375-382.